LAWRENCE
LIVERMORE
NATIONAL
LABORATORY

LLNL-JRNL-647705

Radiochemical Determination of Inertial Confinement Fusion Capsule Compression at the National Ignition Facility

D. A. Shaughnessy, K. J. Moody, N. Gharibyan, P. M. Grant, J. M. Gostic, P. C. Torretto, P. T. Wooddy, B. B. Bandong, C. J. Cerjan, C. A. Hagmann, J. A. Caggiano, L. A. Bernstein, D. H. Schneider, E. A. Henry, R. J. Fortner

December 16, 2013

Review of Scientific Instruments

Disclaimer

LLNL-JRNL-647705

Radiochemical determination of Inertial Confinement Fusion capsule compression at the National Ignition Facility

D.A. Shaughnessy,[1,a)] K.J. Moody,[1)] N. Gharibyan,[1)] P.M. Grant,[1)] J.M. Gostic,[1,b)] P.C. Torretto,[1)] P.T. Wooddy,[1)] B.B. Bandong,[1)] J.D. Despotopulos,[1,2)] C.J. Cerjan,[1)] C.A. Hagmann,[1)] J.A. Caggiano,[1)] C.B. Yeamans,[1)] L.A. Bernstein,[1)] D.H.G. Schneider,[1)] E.A. Henry,[1)] and R.J. Fortner[1)]

[1]*Lawrence Livermore National Laboratory, 7000 East Avenue, Livermore, California, 94551, USA*

[2]*Radiochemistry Program, University of Nevada Las Vegas, Las Vegas, Nevada, 89154, USA*

We describe a radiochemical measurement of the ratio of isotope concentrations produced in a gold hohlraum surrounding an Inertial Confinement Fusion (ICF) capsule at the National Ignition Facility (NIF). We relate the ratio of the concentrations of (n,γ) and (n,2n) products in the gold hohlraum matrix to the down-scatter of neutrons in the compressed fuel and, consequently, to the fuel's areal density. The observed ratio of the concentrations of $^{198m+g}$Au and ^{196g}Au is a performance signature of ablator areal density and the fuel assembly confinement time. We identify the measurement of nuclear cross sections of astrophysical importance as a potential application of the neutrons generated at the NIF.

I. INTRODUCTION

The promise of safe, clean, inexhaustible energy has led to research in controlled fusion methods that could one day be integrated into commercial electrical power supplied. One of the paths toward laboratory scale fusion is Inertial Confinement Fusion (ICF), where a mixture of deuterium and tritium (DT) is compressed to extremely high densities and temperatures by high energy lasers.[1,2] If sufficiently high density and temperature are achieved before the DT target disassembles, the fusion reactions between the two hydrogen isotopes produce alpha particles (^{4}He) that can initiate a self-sustaining burn wave (ignition) in the fuel resulting in more energy being generated than is supplied by the initiating laser beams.[3] The conditions necessary for ignition, and the energy gain factor (defined as the ratio of energy produced to the input laser energy) are both being explored at the National Ignition Facility (NIF), a large-scale, laser-driven ICF complex constructed at the Lawrence Livermore National Laboratory (LLNL).[4]

Even in the absence of an ignition burn, heating and compressing the DT fuel can result in the production of a significant number of neutrons as well as alpha particles. The fraction of thermonuclear fuel that undergoes nuclear reactions is roughly proportional to the product of its density and the time during which compression in maintained (the confinement time). The confinement of the reacting fuel is of limited duration, determined by the inertia compressibility of the fuel mass. Fuel compressions to areal densities greater than 1 g/cm^2 allow an alpha-driven burn wave to be achieved.[5]

a) Author to whom correspondence should be addressed. Electronic mail: shaughnessy2@llnl.gov.

b) Current address: Patrick Air Force Base, Brevard County, Florida, 32925, USA.

The Q-value of the $^{3}H(^{2}H,n)^{4}He$ reaction, which is by far the most probable reaction between hydrogen isotopes at the multi-keV ignition temperature,[6] is 17.6 MeV, and results in the production of neutrons with a narrow energy distribution centered around 14.1 MeV. For a given amount of fuel in the spherical ICF capsule, increased compression results in higher areal density (ρR) and a corresponding increase in the probability for a neutron to scatter off of the residual hydrogen isotopes before it escapes from the fuel. Multiple scattering results in a substantial fraction of the neutrons that escape the fuel being down-scattered to energies between 14 MeV and those associated with keV-thermal temperatures. The neutrons emitted by the imploded capsule (both 14.1 MeV and lower energy down-scattered neutrons) can induce nuclear reactions, and therefore produce radionuclides, in material located in proximity to the capsule. The down-scattered neutrons have fewer reaction pathways energetically available to them than do the 14.1-MeV neutrons, with the lowest-energy fraction producing (n,γ) and (n,n') products. In contrast, the unscattered neutrons produce few capture products, preferentially forming products of threshold reactions, e.g., (n,2n).[7]

The ratio of the concentrations of (n,γ) to (n,2n) products produced in an activation target is related to the fraction of the emitted neutrons that have undergone multiple scattering and is, therefore, related to fuel compression. In the present paper, we report the observation of radioactive nuclei produced in gold targets exposed to the neutron fields generated from ICF capsules and demonstrate the potential diagnostic value of the measurements through a correlation of the (n,γ)/(n,2n) product ratio values with the down-scattered neutron fraction measured by other means.

II. RADIOISOTOPE PRODUCTION IN THE NIF CHAMBER

The ICF capsules used in each experiment consisted of a 2-mm-diameter hollow-shell consisting of germanium-doped, high-density plastic initially filled with a 50:50 mixture of deuterium and tritium gas (the DT fuel) at a pressure of 500-1000 Torr, and subsequently cooled to form a layer of DT ice in the capsule.[8] Each capsule was suspended centrally[9] in a cylindrical metal cavity (the hohlraum), and was maintained at a temperature near the triple point, approximately 19 K, so that a layer of DT ice, which contained most of the mass of the thermonuclear fuel, coated the inside of the shell.[5] The hohlraum, a cylinder roughly 0.6 cm in diameter, 1 cm long, and 30 μm thick (areal density of 0.06 g/cm^2), was constructed of approximately 130 mg of gold, and sometimes contained a small amount of depleted uranium deposited on the inner surface.[10,11] High-Z materials have a high efficiency for conversion of incident laser light to x rays, which drive the capsule implosion. The hohlraum matrix (gold and uranium) constituted the activation target for these diagnostic measurements. The hohlraum was surrounded by a thermal-mechanical package of aluminum approximately 500 μm in thickness, which was

held at the geometrical center of the 10-m-diameter NIF chamber at the end of a boom with clamps containing aluminum and silicon.[12]

Each capsule was imploded by introducing up to 192 beams of 0.35-μm laser light[4,13] through 0.31 cm laser entrance holes located at both ends of the hohlraum. Up to 1.8 MJ of energy were distributed over the inside surface of the hohlraum, which then absorbed the laser light and converted it to x rays.[1,3] The photon energy and time distribution of laser power is tailored to provide an optimal x-ray environment in the hohlraum and to minimize backscattering of the incident laser light and the production of high-energy electrons that could heat the fuel too early, thereby inhibiting compression of the fuel.[14,15,16]

The x-ray bath inside of the hohlraum causes the outer surface of the capsule to ablate, which generates pressure and convergent shocks inside the capsule that compress the DT fuel with high velocity and minimum entropy to the temperatures and densities required for DT fusion. This in turn results in the production of neutrons, and the ρR (areal density) of the capsule ultimately determines the final energy spectrum[3,17,18] of the emitted neutrons. By the time the neutrons are produced, most of the plastic shell has ablated away, and the majority of the neutrons emerging at lower energies arise from scattering off of the isotopes of hydrogen in the fuel together with a significant contribution from the hydrogen in the remaining plastic ablator. Contributions from the low-density plasma that fills the hohlraum are negligibly small.

At maximum compression, the diameter of the hottest portion of the DT fuel (the hot spot) inside the capsule approaches 40 μm and the ρR of the cold fuel approaches 1 g/cm^2 (reference 19). The time between the onset of the laser pulse and the production of neutrons is sufficiently short (nanoseconds)[20] that there is very little motion of the bulk gold hohlraum material from its initial position during that time even though a few micrometers of its inner surface have been heated to hundreds of eV.[17] The neutrons arrive at the hohlraum and produce a variety of nuclear reaction products before the hohlraum matrix finally breaks apart and moves away from the center of the NIF chamber, thereby becoming target "debris". Of the energy produced in the fusion process, 80% is in the motion of the neutrons, which pass through the hohlraum without depositing much energy. For capsules with yields below those associated with ignition, most of the propulsion of capsule and hohlraum debris is due to laser heating rather than nuclear processes. Following neutron production, high-kinetic-energy ICF-capsule material stagnates against the hot inner wall of the hohlraum, launching shocks into the matrix. When the shocks break out of the outer surface of the hohlraum, much of the energy is radiated as part of the x-ray continuum, but the rest goes into kinetic energy of the debris.[21] This leads to atom-scale surface vaporization and larger-size ejecta from impulse loading and subsurface boiling, which propagate ballistically through the vacuum of the NIF chamber shortly after leaving the vicinity of the center of energy production.[22,23,24,25] The majority of the hohlraum mass is expected to be directed axially outward.[26,27]

In these experiments we fielded passive collector foils at a distance of 50 cm from the target chamber center (TCC) to collect the resultant capsule and hohlraum debris. These collectors were oriented near the plane of symmetry through the cylindrical waist of the hohlraum so as to maximize the collection of gold activation products. The collection process is complicated by the harsh environment found inside the NIF chamber following a shot, which includes scattered laser light, x rays, neutrons, and debris that originated from material ablated from the chamber wall and diagnostic instruments fielded inside the chamber. Neutrons emitted by the DT fuel and x rays emitted by the hohlraum and thermal-mechanical package arrive at the collector position approximately 10 ns following the end of fusion-energy production. Debris arrives considerably later, on the order of microseconds to milliseconds depending on the size and mass of the particulates. The sub-keV x rays that dominate the spectrum of photons emitted by the hohlraum assembly deposit most of their energy within a few micrometers of the surface of high-melting point collector materials.[28,29] The x-ray pulse duration was short compared to the time required for heat transport,[30] so surfaces were driven past their melting points (see reference 31, for example.) The associated thermal shock caused material to ablate from the surface of the collector, which could impeded the arrival of atom-scale debris. This problem is expected to be worse if the collector is moved from a waist, or equatorial, location to a polar location; the spectrum of radiation emitted through the laser entrance holes at the ends of the hohlraum was of higher energy,[21,32] which added significantly to the x-ray load on the polar collectors. Gamma-ray spectroscopic analyses of the gold on the collector foils indicated clearly that the gold debris was not homogenously distributed with respect to the pole and equator. These analyses also showed that the distribution of gold debris at the equatorial line-of-site varied significantly for a given shot, with no dependence on the collector material, bracket position, or laser energy.[28]

The energy spectrum of neutrons that have passed through the hohlraum is measured at NIF by a magnetic recoil spectrometer (MRS)[33] and a variety of scintillator-based neutron time-of-flight (NTOF) detectors.[34,35,36,37] These diagnostics have limited sensitivities to neutrons with "low" energies (the lower-energy thresholds are 140 keV for NTOF and 4 MeV for MRS.) A typical NTOF spectrum is shown in Figure 1, and typical derived neutron energy spectra for two ρR values are shown in Figure 2. One quantity that is derived from the measured spectra is the down-scattered neutron ratio (DSR), which is used to infer the ρR of the fuel.[38] DSR is defined as the number of neutrons that have energies between 10 and 12 MeV (most of which have scattered only once) divided by the number of neutrons considered to be "unscattered", with energies between 13 and 15 MeV. In this work the DSR of the capsule was obtained by fitting the neutron energy spectra from the two 20-meter NTOF detectors and from the MRS, 10-12 MeV and 13-15 MeV, respectively, and calculating the ratio. The authorized DSR value for each NIF shot is determined by performing a weighted average of DSR values from several neutron diagnostics.

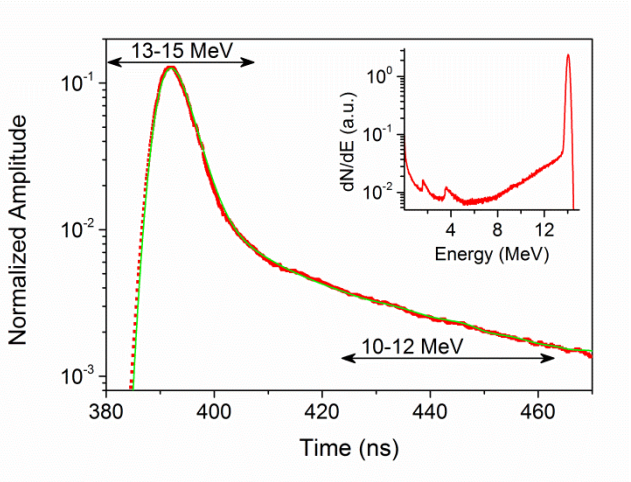

FIG. 1. Neutron Time-Of-Flight (NTOF) spectrum from the equatorial NTOF 20 meter detector for shot N120321-001-999. The red dots are data with error bars; the green line is the fit to the data. Inset is the energy spectrum used to fit the data, from an MCNP simulation. The DSR inferred from this spectrum is 0.050 ± 0.004 and the average over all lines-of-site is 0.060 ± 0.004. This deviation from the average is consistent with a systematic low DSR on the equator for cryogenic fuel implosions.

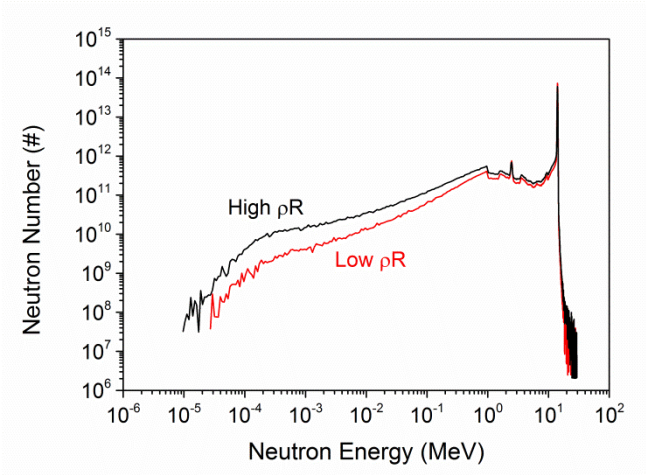

FIG. 2. Post-shot analysis of the neutron number escaping the capsule boundary, plotted as a function of energy. The spectra are derived from NIF implosion experiments N111215 (Low-ρR) and N120321 (High-ρR), which had measured DSR values of 0.046 and 0.062, respectively. These DSR values correspond to DT areal densities of 0.92 and 1.24 g/cm^2.

Neutrons emitted by the NIF capsule also encounter the NIF chamber wall and the various structural supports located relatively close to the center of fusion-energy production. The neutrons scattered off these materials bathe the region near the center of the NIF chamber with lower-energy "room-return" neutrons. Room-return neutrons include those resulting from (n,2n) reactions on local target support and diagnostic structures, as well as the more highly thermalized neutrons scattered from chamber walls and surrounding building materials. The interaction of these neutrons with the hohlraum debris, mostly through (n,γ) reactions, must be assessed before the ^{197}Au(n,γ) products can be attributed primarily to the capture of neutrons that had previously down-scattered solely off the fuel in the compressed ICF capsule.[39] A Monte Carlo neutron transport calculation using MCNP5 with ENDF/B-VII.0 cross sections was performed to assess the contribution of room-return neutrons.[40] The main components of the NIF target chamber and surrounding building were included in the Monte Carlo

geometry. Isotropic DT fusion neutrons were injected at the center of the chamber and tracked until they either escaped or were captured in the building materials. Gold activation tallies were calculated at various radii from the center. The contribution from room return was evaluated by subtracting the activation by the bare capsule. Figure 3 shows the simulation results indicating that room return neutrons make a negligible contribution to the gold ratio for distances < 1 cm, even for low ρR capsules. We performed the experiments described below to verify the results of these simulations.

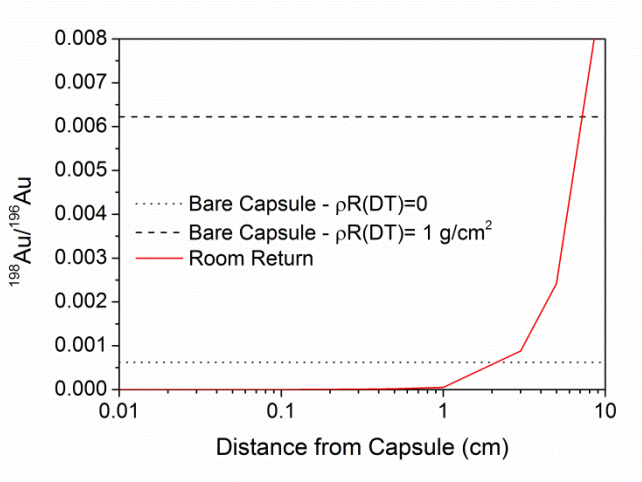

FIG. 3. Calculated Au isotope ratio N(^{198}Au)/N(^{196}Au) from unscattered and room return neutrons as a function of distance from the center of the NIF target chamber. The neutron source is a pure DT fusion spectrum at an ion temperature of approximately 3 keV. The expected Au ratio for two different values of ρR(DT) is also shown for comparison. A thin Au absorber with negligible neutron down-scatter is assumed.

III. NEUTRON REACTIONS ON ^{197}Au

The radioisotope inventory arising in fast-neutron interactions with ^{197}Au is dominated by the products of (n,2n) and (n,γ) reactions, forming ^{196}Au and ^{198}Au, respectively. Both ^{196}Au and ^{198}Au have long-lived isomeric states that decay by internal conversion.[41,42,43] The 8.2-second first isomeric state in ^{196}Au has completely decayed to the 6.2-day ground state before our radiometric measurements could be performed due to the length of time associated with retrieving collectors following a NIF shot; isotopic concentrations that we attribute to ^{196g}Au are more accurately associated with the sum of those for ^{196m1}Au and ^{196g}Au. We refer to the higher-energy 9.6-hour isomeric state with the short-hand designation ^{196m}Au for the following discussions.

The nuclear level structures of ^{196}Au and ^{198}Au are very similar, with long-lived $J^{\pi}=12^-$ isomeric states lying at substantial excitation energies over $J^{\pi}=2^-$ ground states. In ^{196}Au, the 9.6-hour isomer is at an excitation energy of 596 keV above the 6.2-day ground state. In ^{198}Au, the 2.3-day isomer is at an excitation energy of 812 keV above the 2.7-day ground state. Both isomeric states decay by a series of electromagnetic transitions to their respective ground states. The ground state

of ^{198}Au decays by β emission. The ground state of ^{196}Au decays mainly by electron capture (EC), but there is a 7% β^- branch.

The ^{197}Au(n,2n) reaction has a threshold of 8.1 MeV.[44] This means that scattered room-return neutrons are unlikely to contribute to the production of ^{196}Au. For neutrons with energies in the vicinity of 14.1 MeV, the cross section for the production of $^{196m+g}$Au is 2200 mb[45] (see Figure 4). The target nuclide ^{197}Au has $J^{\pi}=3/2^{+}$; the required spin change and the excitation energy of ^{196m}Au strongly favors the production of the ground state. The average of literature values for the isomer ratio is $\sigma(^{196m}\text{Au})/\sigma(^{196g}\text{Au})=0.069$,[46,47,48,49] which is nearly identical to the value we obtained from our measurements (see results below).

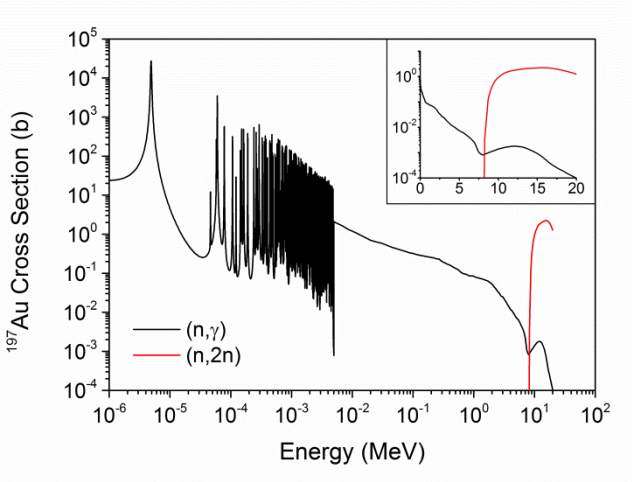

FIG. 4. ^{197}Au(n,2n) and ^{197}Au(n,γ) evaluated cross sections from the Evaluated Nuclear Data File available through the National Nuclear Data Center at Brookhaven National Laboratory[50]. The inset figure has the Au cross sections with a linear scale for the neutron energy.

The ^{197}Au(n,γ) reaction has no energy threshold; therefore, neutrons of all energies can produce ^{198}Au (see Figure 4). Due to the similarity of the ^{198}Au and ^{196}Au nuclear structures, it may be possible that a similar isomer ratio would be obtained with 14-MeV-neturon capture as for the (n,2n) process. The ^{197}Au(n,γ) cross section at 14 MeV is only 1 mb,[39,51,52] yet we observe production of ^{198}Au considerably in excess of that which would be produced with this cross section (see results below). This is a consequence of the contribution from reactions with neutrons of lower energy. Less angular momentum and excitation energy are contributed to the compound nucleus in these lower-energy capture reactions, resulting in a substantially lower isomer ratio. We did not obtain any conclusive evidence for the production of ^{198m}Au in the present experiments.

IV. EXPERIMENTAL DETAILS

The Solid Radiochemistry (SRC) debris collectors were fielded in the NIF chamber on a fixed bracket mounted on the outside surface of a retractable Diagnostic Instrument Manipulator (DIM)[53] (see Figure 5). The distance between the center of the front surface of the collector disk and the center of the ICF capsule was 50 cm, with the line of site being very nearly perpendicular to the surface of the disk. In several instances, trailing thin foils were mounted behind the collector disks so that they were not exposed to the chamber debris, but were exposed to the neutron flux leaving the capsule plus the room return neutrons. Each collector foil stack was backed up against a compression spring such that the collecting surface always registered against the retaining clamp at exactly the same distance from the ICF capsule.

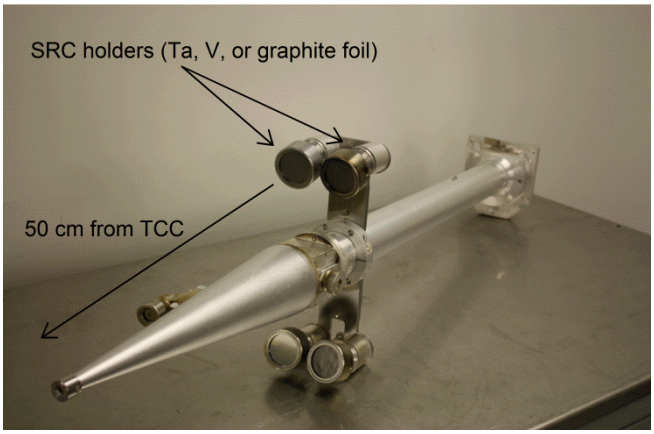

FIG. 5. A picture of the snout, which attaches to the end of the Diagnostic Instrument Manipulator (DIM), with four Solid Radiochemistry (SRC) collector holders in place. The ICF target assembly at the target chamber center (TCC) is just beyond the end of the snout, 50 cm from the SRC holders.

A variety of materials with at least 99.9% purity were employed as collectors, including Ta, V, Ti, Nb, Mo, Ag, and graphite foil; these were part of a systematic effort to determine the relative collection properties of the materials. Each collector was 5 cm in diameter and 1 mm thick, with the exception of the graphite foil, which was 0.1 mm thick and backed with a 0.5 mm thick piece of aluminum. A variety of surface finishes were also explored, and it was determined that polished surfaces with a roughness of ≤ 1 μm rms variation were most effective in debris collection. The retaining ring that held the collector in position was stainless steel, with an opening that was 4 cm in diameter; while the entire volume of the collector foil was activated by the neutron exposure, only a 4-cm-diamterer area centered on the front of the disk collected debris (4×10^{-4} of 4π solid angle). There was little systematic advantage of any particular material over the others in the efficiency of debris collection,[28] but Ta, V, and graphite foil provided the least interference with the detection of gamma rays emitted by the gold-hohlraum material. In some of the experiments whose results are given below, Ta collectors (~1.7 g/cm^2) were backed with an Al isolation foil, a Au disk, and a Ta disk, each 0.1 mm thick (see Figure 6); these trailing foils were designed to measure room-return neutrons. The cross section for the elastic scattering of fast neutrons by high-Z materials is on the

order of a few barns, giving an inverse cross section of 0.5 mole/cm^2. A 1-mm-thickness of most metals is on the order of 0.01 mole/cm^2, so there are few down-scatter interactions of neutrons as they pass through the foil stack.

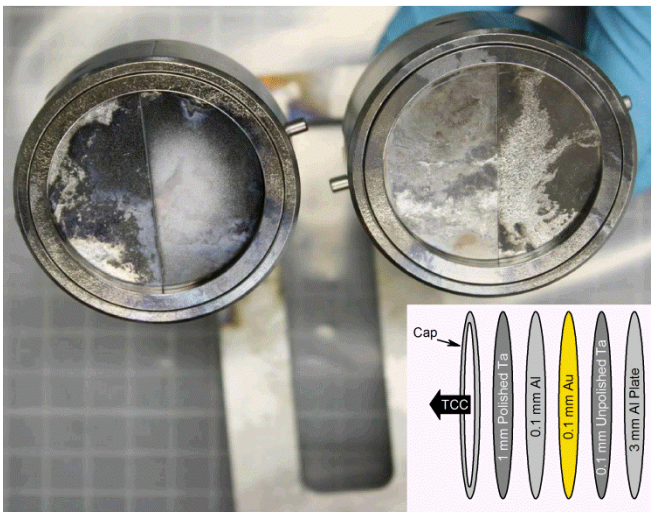

FIG. 6. A post-shot picture and schematic drawing of the debris collectors, oriented toward the target chamber center (TCC), fielded in one of the NIF shots. The pre-shot collector foils were polished to a surface finish of ≤ 1 μm rms; the surface discoloration is due to the effects of radiation and debris from the lasers, hohlraum, and NIF capsule. Each collector is typically 5 cm in diameter and 1 mm thick, with the exception of the graphite foil, which is 0.1 mm thick and backed with a 0.5 mm thick piece of aluminum.

Samples were retrieved from the NIF chamber and were available for gamma-ray counting between 3 and 12 hours following the laser shot. The samples were wrapped in two layers of plastic to contain adsorbed tritium, which was present in the NIF chamber as unconsumed fuel from the ICF capsule. They were then mounted in standard aluminum or plastic counting fixtures, covered with precisely machined cadmium foils (0.4 g/cm^2) and placed at well-characterized locations in front of high-purity germanium coaxial photon detectors[54] in shielded enclosures. The purpose of the cadmium foils was to absorb the platinum x rays emitted in the EC decay of ^{196g}Au so that they would not sum in the detector material with the coincident gamma rays; for photons with energies above 100 keV, the attenuation was < 50%.[55] The detectors had relative efficiencies between 20% and 40% of a reference sodium-iodide detector, NaI(Tl).[54] The energy and efficiency calibrations were performed[56] with NIST-traceable radionuclide certified reference materials in accordance with the International Organization for Standardization (ISO) 17025 standard.

Each collector was counted several times over a span of three or more days. Initially, several 4-hour counts of each source were taken to characterize the intensities of the gamma rays emitted by 9.6-hour ^{196m}Au. The source was placed no closer than 3 cm from the front face of the detector end cap in order to minimize coincident summing, since a cascade of photons are emitted in the decay of ^{196m}Au. Afterward, the source was moved 2 cm closer to the detector and counted to quantify the 2.3-day ^{198g}Au and the ^{196g}Au β branch, which do not suffer from summing. Two days after the shot, the source

was backed off to its original position to quantify the 6.2-day ^{196g}Au. In each case, the count rate in the detectors was sufficiently small that no correction was necessary for random summing.

Photon spectra between 50 keV and 2 MeV were collected in 4096 channels. The time base was corrected internally for dead time. The spectra were processed with LLNL's GAMANAL code,[57,58] which calculated the energy and intensity of each observed photon peak using the calibration parameters (including peak shape); it also corrected for extended source size and attenuation due to the presence of the plastic confinement layers, the cadmium absorber, and self-attenuation by the sample iself.[55] Uncertainties associated with the final photons/minute data were obtained from the statistical weights of the photopeaks and algorithms in the code taking into account photopeak efficiencies. In rare cases where a desired photopeak was insufficiently intense to be quantified by GAMANAL, its intensity and associated uncertainty were determined graphically. Each spectrum was processed through GAMANAL twice, once as a 5-cm-diameter x 1-mm-thick disk for the calculation of the intensities of activities induced by neutrons in the collector matrix, and a second time as a 4-cm-diameter by 1-μm-thick disk for the calculation of the intensities of activities collected on the foil surface. The assumption of a 1-μm-thick distribution of debris is based on measurements of the melt depth in cross-sectioned Ta and V collectors;[28] the associated attenuation correction was a small addition to that for the cadmium absorber. Based on the absolute count rates from the various collectors, there is evidence that the solid debris that emanates from the NIF capsule and hohlraum assembly is not distributed homogenously in the lateral direction. Therefore, we report isotope ratios as a means to mitigate the effects of uneven debris collection on the collector surfaces.

In the debris-collector spectra we routinely observed the photons emitted in the decays of ^{196m}Au, ^{196g}Au, and ^{198g}Au. We also observed photons associated with interfering activities produced in the collector matrix itself, as well as ^{24}Na, which we attribute to ^{27}Al(n,α)^{24}Na reactions in the thermal-mechanical package surrounding the hohlraum. We have no convincing evidence for the observation of ^{198m}Au, and placed an upper limit of 0.11 to 0.13 on the ^{198m}Au/^{198g}Au ratio for several representative samples. In the trailing gold foils we also detected ^{196m}Au, ^{196g}Au, and ^{198g}Au. The limit on the production of ^{198m}Au in these foils was $N(^{198m}Au)/N(^{198g}Au) \leq 0.002$.

Photon intensity information from GAMANAL was converted to atoms at shot time using evaluated nuclear data,[41,42,43] summarized in Table I. The number of atoms was obtained by dividing the photon intensities by the product of the overall normalization and the gamma-ray relative intensity. For nuclide species that emit several intense gamma rays, the number of atoms was determined using each gamma ray and the results were averaged. The reference time associated with the intensity of each measured photopeak was near the centroid of the counting interval, corrected for the nonlinearity of the decay during that interval (finite-counting-time correction).[57] The photopeak intensities associated with each observed activity were

calculated at the time of the shot assuming a single-component exponential decay. Several determinations of the initial concentrations of the same nuclide were propagated as a weighted average. We corrected the resulting initial atom concentration of ^{196g}Au for contributions from the decay of ^{196m}Au under the asymptotic assumption: By using ^{196g}Au data taken after 48 hours of decay, given the isomer ratio from the literature, we can assume that the decay of ^{196m}Au is sufficiently complete that simple exponential decay of ^{196g}Au has been established (within 0.3%). Under this condition, the difference between the single-component extrapolation to shot time and the actual initial concentration of ^{196g}Au is $\lambda(^{196m}\text{Au})/[\lambda(^{196m}\text{Au})-\lambda(^{196g}\text{Au})] \times N(^{196m}\text{Au})$, or 1.0694 times the measured initial isomer concentration. We assumed that the production of ^{198m}Au was negligible, and made no correction for its decay contribution to the extrapolated initial concentration of ^{198g}Au.

TABLE I. Nuclear data for gold isotopes, used to convert observed photon intensities to atoms at shot time.[41,42,43]

Nuclide	Half-life (min)	Normalization	Photon energy (keV)	Relative intensity
^{196g}Au (EC)	8880.3(9)	0.869(9)	333.0	0.263(6)
			355.7	1.000
^{196g}Au (β)	8880.3(9)	0.066(3)	426.1	1.000
^{196m}Au	576(6)	0.087(3)	147.8	5.00
			168.4	0.90(5)
			188.3	3.45(12)
			285.5	0.51(5)
			316.2	0.34(3)
^{198g}Au	3880.4(4)	0.9558(12)	411.8	1.000
^{198m}Au	3271.7(23)	0.77(1)	97.2	0.90(4)
			180.3	0.63(5)
			204.1	0.51(4)
			214.9	1.000

More than one collector foil were fielded on many of the ICF shots whose results are presented below. The gamma-ray data from each collector were processed individually to derive an isotope ratio for that foil. The debris collection efficiency was quite variable among the foils. The uncertainties associated with the intensity of the photon lines emitted in the decay of the gold debris were dependent on the efficiency, the activation of the collecting medium, and the time required to recover

the sample from the NIF target chamber and to mount it for counting. As a result, for each ICF shot, it was quite common that one sample yielded a N(^{198g}Au)/N(^{196g}Au) value (the isotope ratio) that was of significantly lower uncertainty than those yielded by the other collectors. Rather than propagate together all the isotope ratio values from one shot, we report the best value for an individual collector; the other values were treated as confirmatory and are not presented here.

The down-scattered neutron ratio was determined from the neutron energy spectrum measured by two types of diagnostic devices. The first consists of NTOF instruments[59] located approximately 20 m from TCC, and oriented in the equatorial and polar directions with respect to the hohlraum. These instruments detect the neutrons using a fast xylene scintillator with a low scintillation tail at greater than 40 ns after the main scintillation peak. The other neutron diagnostic device, the MRS,[60] determines the neutron energy by measuring recoil protons produced by neutrons colliding with a thin plastic foil. These protons are magnetically analyzed and focused on a series of collectors that record the protons using CR-39 (Columbia Resin #39) film. The authorized DSR value for a particular laser shot is determined using the suite of neutron spectral measurement devices active on that shot. The number of neutrons in the two energy bins is determined for each instrument and the ratio formed. The ratios from the active devices are averaged to determine the authorized DSR value.

V. RESULTS

From an MCNP simulation, we expected the correction for the contribution of room-return neutrons (neutrons thermalized through scatterings from the NIF experimental apparatus and the chamber walls) to the ^{198}Au content of the hohlraum debris to be small (see Figure 3). Before the shot, the average distance of the Au hohlraum is approximately 0.37 cm from the capsule and little motion is expected before burn time. From the results of Figure 3, we predict a small contribution from room return to the Au ratio. Nevertheless, we performed activation measurements to evaluate this conclusion guided by the calculation. In four cases in which a Ta collector was employed, we backed the collector with thin foils of Au and Ta. These foils were retrieved and counted separately from the collector foil. Sections of representative spectra from one experiment are shown in Figure 7. All three spectra were taken at approximately the same time with detectors of similar efficiencies. The top spectrum is associated with the trailing Au foil, the middle spectrum is a count of the debris collector (Au collected on Ta), and the bottom spectrum is associated with the trailing Ta foil. From the comparison of the bottom and middle spectra, it is clear that the activation of Ta does not interfere with the detection and quantification of gold hohlraum debris.

Inspection of the top and middle spectra in Figure 7 show that there is a substantial contribution from the capture of room-return neutrons to the ^{198}Au concentration in the trailing gold foil compared to that in the hohlraum material. Quantitatively, the measured N(^{198}Au)/N(^{196}Au) isotope ratio in the trailing foil is 11 ± 4 times greater than in the hohlraum

material. We assume that the room-return neutron field produced by scatter from the chamber walls and experimental fixtures and equipment in the chamber is essentially the same for both the trailing foil and the hohlraum material because of their proximity in the large NIF chamber. However, the exposure to neutrons produced in the capsule decreases with the square of the distance from the capsule. The hohlraum is 1 cm in diameter and is approximately 0.37 cm from the capsule when the fusion neutrons arrive, while the trailing foil is 50 cm from the capsule. Since the measured N(^{198}Au)/N(^{196}Au) isotope ratio in the trailing gold foil is about 11 times greater than what was measured in the gold hohlraum debris, we can approximate that the room-return neutrons contribute about $11/(50)^2$ (where 50 is the distance in centimeters from the capsule to the trailing foil), or less than 1%, to the production of ^{198}Au in the hohlraum debris. This is corroborated by the MCNP calculation shown in Figure 3, which indicates that at the edge of the hohlraum (1 cm) the contribution from room return neutrons is negligible. As a result, we assess the measured N(^{198}Au)/N(^{196}Au) isotope ratio in the debris as arising from the interaction of the capsule neutron output with the gold-hohlraum matrix without significant contribution from room return.

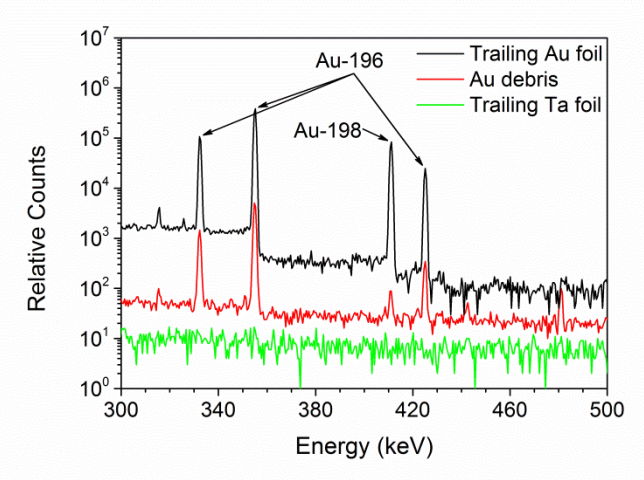

FIG. 7. Spectra of gamma rays from hohlraum gold debris collected on a Ta collector disc and trailing foils from a representative NIF shot. The top line is the spectrum from the thin Au foil placed behind the Ta collector, the middle line is the spectrum of the gold hohlraum debris that was collected on the Ta collector, and the bottom line is the spectrum from the thin Ta foil placed behind the collector and trailing Au foils (see Figure 6 for collector schematic.)

In Table II we present the results of our radiochemical measurements of the N(^{198}Au)/N(^{196}Au) ratios from debris collectors from 17 ICF shots fielded between January 2012 and March 2013, correlated with the authorized DSR value associated with each experiment. These data are presented graphically in Figure 8.

The N(^{196m}Au)/N(^{196g}Au) ratio has been measured for 18 ICF shots utilizing gold spectroscopic data from hohlraum debris collected near the equatorial plane. The data are summarized in Table II along with isomer ratios reported in the literature. The literature values vary considerably, ranging from 5.9% to 7.9%, with an overall average of 6.9%. The isomer

TABLE II. Experimental N(^{198}Au)/N(^{196}Au) isotope and N(^{196m}Au)/N(^{196g}Au) isomer ratios, along with the DT neutron yield and the authorized DSR (with one sigma uncertainty intervals) from 18 ICF shots (identified with a six-digit number giving the shot year, month, and day). Isotope ratios (with statistical uncertainties) are from the analyses of the front collector disks. Systematic uncertainties for the isotope and isomer ratios are 4.0% and 1.1%, respectively.

NIF shot ID	DT neutron yield (x 10^{14})	DSR (x 10^{-2})	N(^{198}Au)/N(^{196}Au) (x 10^{-3})	N(^{196m}Au)/N(^{196g}Au) (%)
N120126	3.18	3.92 ± 0.16	8.39 ± 1.96	8.02 ± 0.69
N120131	6.19	3.67 ± 0.17	7.12 ± 0.38	7.10 ± 0.16
N120205	5.64	4.30 ± 0.19	8.66 ± 0.31	7.23 ± 0.12
N120213	0.97	4.25 ± 0.24	7.88 ± 6.22	6.77 ± 0.40
N120219	3.51	4.33 ± 0.17	8.68 ± 0.60	7.55 ± 0.27
N120311	1.30	4.97 ± 0.30	12.9 ± 3.37	7.76 ± 0.71
N120316	2.18	5.80 ± 0.32	18.7 ± 2.11	6.81 ± 0.43
N120321	4.20	6.26 ± 0.46	22.5 ± 1.73	6.91 ± 0.44
N120405	1.28	5.14 ± 0.29	12.2 ± 1.54	7.03 ± 0.35
N120412	1.05	6.25 ± 0.33	32.3 ± 12.0	6.33 ± 0.96
N120417	4.30	5.32 ± 0.21	16.7 ± 0.46	6.96 ± 0.11
N120626	0.99	4.55 ± 0.22	NM	6.73 ± 0.87
N120716	2.40	5.25 ± 0.22	18.3 ± 3.4	6.62 ± 0.69
N120720	1.50	6.13 ± 0.34	24.9 ± 5.0	6.91 ± 0.66
N120802	3.03	4.46 ± 0.22	9.11 ± 0.37	6.88 ± 0.11
N120808	1.52	4.67 ± 0.40	16.1 ± 0.95	7.02 ± 0.24
N120920	4.75	4.01 ± 0.28	11.7 ± 3.7	7.20 ± 0.24
N130331	2.96	4.12 ± 0.20	8.04 ± 2.26	7.04 ± 0.26
Wtd Average				7.05 ± 0.04
Ref. 46				5.9 ± 0.4
Ref. 47				6.8 ± 0.8
Ref. 48				7.9 ± 0.8
Ref. 49				6.8 ± 0.3
Unwtd Average				6.9

ratios obtained from the gold samples produced via irradiation from ICF capsule neutrons are consistent with each other within statistical accuracy, and an overall weighted average of 7.05 ± 0.04% (statistical uncertainty) is obtained, which appears to be an improvement over the currently reported values.

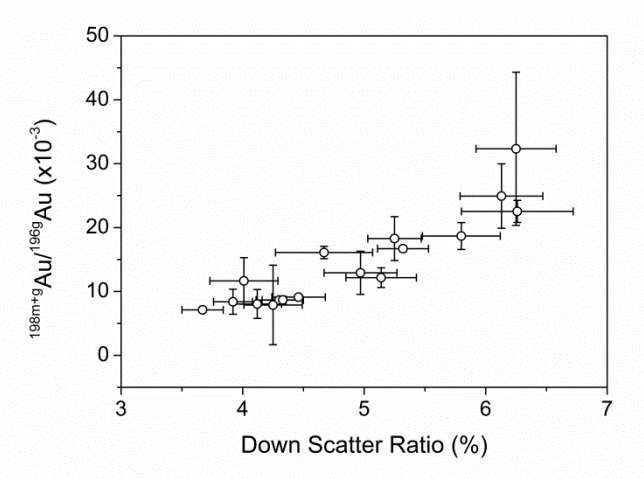

FIG. 8. A plot of the Au isotope ratio N($^{198m+g}$Au)/N(^{196g}Au) versus the DSR value from the NIF shots presented in Table II. One sigma error bars are plotted.

VI. DISCUSSION

The ratio of ^{197}Au(n,γ) and ^{197}Au(n,2n) cross sections at 14 MeV is approximately $5x10^{-4}$ (see Figure 4). We observe that in each case listed in Table II the N(^{198}Au)/N(^{196}Au) value is in excess of this, demonstrating the contribution to ^{198g}Au production from capsule neutrons at energies well below 14 MeV. Figure 8 demonstrates that the correlation between the gold isotope ratio and the DSR is monotonically increasing, though not linear, since for a monoenergetic 14-MeV neutron spectrum the isotope ratio at DSR=0 should be approximately $5x10^{-4}$. In reality, additional captures of lower energy DD and TT fusion neutrons and neutrons down-scattered in the hohlraum bring the expected DSR=0 ratio up to about $1x10^{-3}$. The non-linearity of the gold isotope ratio data is not surprising because the DSR is a measure of neutrons that have undergone a very limited number of scattering interactions, while the production of the ^{198g}Au component of the gold isotope ratio is strongly influenced by exposure to more highly scattered neutrons (see Figure 4). Despite this observation, the gold isotope ratio versus DSR value can be represented approximately by a straight line over the present range of the data.

The DSR and gold ratio provide information about compression (ρR) of the fuel (DT) and plastic capsule ablator (CH) during burn. Nuclear cross sections at E = 14 MeV show that for a given ρR, the DSR contribution from DT is about four times that of CH. By contrast, DT and CH are approximately equally effective in increasing the gold ratio through neutron

down-scattering. A given pair of DSR and gold ratio values can therefore be used to uniquely determine both ρR(DT) and ρR(CH) at burn time. Details of the analysis and application to NIF data will be given in a separate paper.

The gold isomer ratios, $N(^{196m}Au)/N(^{196g}Au)$, from the individual shots are consistent with each other within the uncertainties of the measurement, as well as the extant literature data (see Table II). There is no significant dependence of the values on the 14-MeV neutron yield or DSR for these data obtained from collectors located equatorially. The weighted average obtained, 7.05 ± 0.04% (statistical) ± 0.28% (systematic), is in good agreement with the isomer ratios determined from accelerator-based measurements. Experiments such as these at the NIF have an advantage that all radioactive species are produced at essentially the same instant.

The success of these nuclear isotope and isomer ratio measurements at the NIF suggests that the facility can be used for studies in basic nuclear physics and astrophysics. The fuel in an ICF capsule is driven to temperatures and pressures comparable with those found in the interiors of Asymptotic Giant Branch (AGB) stars, low- to medium-mass stars where the s-process is thought to occur. This nucleosynthesis process occurs over a long time period by capture of neutrons generated by the nuclear reactions in the star. Depending on the mass, composition, and stage of evolution of the AGB star, the s-process produces elements heavier than Fe up to Y and Sr, even up to Pb under some conditions. These heavy elements can be ejected into the interstellar medium by a supernova explosion.

Although the neutron spectrum produced by an ICF capsule is dominated by 14-MeV neutrons (see Figures 1 and 2), there can be a significant contribution from neutrons that mimic those that produce heavy elements via the s-process.[61,62,63] In addition, since the thermal environment during the ICF implosion is elevated, the potential exists to measure cross sections of nuclei with excited levels in thermal equilibrium, an interesting complement to experiments at accelerator laboratories where targets are at ambient temperature.

Mounting collection assemblies with trailing foils at more than one distance from the NIF target-chamber center can be used to distinguish that fraction of an induced isotope inventory due to room return from that arising directly from the capsule. If the spectrum of room-return neutrons can be characterized, intensities are such that radiochemical measurements of cross sections for (n,γ) reactions at intermediate energies can be proposed.

In summary, measurements of the neutron activation of gold in the hohlraum of NIF ICF capsules have been performed to demonstrate the usefulness of these measurements to diagnose ICF implosions, as well as to measure neutron cross sections or cross section ratios. Furthermore, since the ICF implosions occur at temperatures comparable to those in stars, the possibility to use NIF to measure neutron cross sections of importance to astrophysics is suggested by the present work.

ACKNOWLEDGMENTS

The authors would like to thank the NIF Nuclear Diagnostics Group and NIF Engineering and Operations staff, in particular, Richard Zacharias, Kenn Knittel, Christopher Wlodarczyk, Justin Wright, Bowdi Helgesen, Glenn Grant, Tim Cunningham, Wayne Abreu, James Daly, Bahram Talison, and the NIF Radiation Control Technicians. This work was performed under the auspices of the U.S. Department of Energy by Lawrence Livermore National Laboratory under Contract DE-AC52-07NA27344.

REFERENCES

[1]J.H. Nuckolls, Phys. Today **35**, 24 (1982).

[2]J. Nuckolls, L. Wood, A. Thiessen, and G. Zimmermann, Nature **239**, 139 (1972).

[3]J. Lindl, Phys. Plasmas **2**, 3933 (1995).

[4]E.I. Moses, R.N. Boyd, B.A. Remington, C.J. Keane, and R. Al-Ayat, Phys. Plasmas **16**, 041006 (2009).

[5]J.K. Hoffer and L.R. Foreman, Phys. Rev. Lett. **60**, 1310 (1988).

[6]R.F. Post, Ann. Rev. Nucl. Sci. **20**, 509 (1970).

[7]V. McLane, C.L. Dunford, and P.F. Rose, *Neutron Cross Sections, Volume 2, Neutron Cross Section Curves* (Academic Press, Boston, 1988).

[8]S.W. Haan, J.D. Lindl, D.A. Callahan, D.S. Clark, J.D. Salmonson, B.A. Hammel, L.J. Atherton, R.C. Cook, M.J. Edwards, S. Glenzer, A.V. Hamza, S.P. Hatchett, M.C. Herrmann, D.E. Hinkel, D.D. Ho, H. Huang, O.S. Jones, J. Kline, G. Kyrala, O.L. Landen, B.L. MacGowan, M.M. Marinak, D.D. Meyerhofer, J.L. Milovich, K.A. Moreno, E.I. Moses, D.H. Munro, A. Nikroo, R.E. Olson, K. Peterson, S.M. Pollaine, J.E. Ralph, H.F. Robey, B.K. Spears, P.T. Springer, L.J. Suter, C.A. Thomas, R.P. Town, R. Vesey, S.V. Weber, H.L. Wilkens, and D.C. Wilson, Phys. Plasmas **18**, 0551001 (2011).

[9]S.O. Kucheyev and A.V. Hamza, J. Appl. Phys. **108**, 091101 (2010).

[10]H.L. Wilkens, A. Nikroo, D.R. Wall, and J.R. Wall, Phys. Plasmas **14**, 056310 (2007).

[11]O.S. Jones, J. Schein, M.D. Rosen, L.J. Suter, R.J. Wallace, E.L. Dewald, S.H. Glenzer, K.M. Campbell, J. Gunther, B.A. Hammel, O.L. Landen, C.M. Sorce, R.E. Olson, G.A. Rochau, H.L. Wilkens, J.L. Kaae, J.D. Kilkenny, A. Nikroo, and S.P. Regan, Phys. Plasmas **14**, 056311 (2007).

[12]G.J. Laughon and K.R. Schultz, Fusion Technol. **30**, 471 (1996).

[13]R.S. Craxton, Optics Commun. **34**, 474 (1980).

[14]T. Chang, J. Sheng, W. Miao, Y. Li, S. Jiang, W. Pei, J. Chen, Y. Gao, J. Yang, T. Feng, Z. Zheng, L. Zhang, Y. Ding, J. Li, and M. Li, Phys. Plasmas **13**, 022704(2006).

[15]L. Suter, J. Rothenberg, D. Munro, B. van Wonterghem, and S. Haan, Phys. Plasmas **7**, 2092 (2000).

[16]K.A. Brueckner and S. Jorna, Rev. Mod. Phys. **46**, 325 (1974).

[17]J.D. Lindl, *Inertial Confinement Fusion, The Quest for Ignition and Energy Gain Using Indirect Drive* (AIP Press/Springer-Verlag, New York, 1998).

[18]S.E. Bodner, J. Fusion Energy **1**, 221 (1981).

[19]A.J. Mackinnon, J.L. Kline, S.N. Dixit, S.H. Glenzer, M.J. Edwards, D.A. Callahan, N.B. Meezan, S.W. Haan, J.D. Kilkenny, T. Döppner, D.R. Farley, J.D. Moody, J.E. Ralph, B.J. MacGowan, O.L. Landen, H.F. Robey, T.R. Boehly, P.M. Celliers, J.H. Eggert, K. Krauter, G. Frieders, G.F. Ross, D.G. Hicks, R.E. Olson, S.V. Weber, B.K. Spears, J.D. Salmonsen, P. Michel, L. Divol, B. Hammel, C.A. Thomas, D.S. Clark, O.S. Jones, P.T. Springer, C.J. Cerjan, G.W. Collins, V.Y. Glebov, J.P. Knauer, C. Sangster, C. Stoeckl, P. McKenty, J.M. McNaney, R.J. Leeper, C.L. Ruiz, G.W. Cooper, A.G. Nelson, G.G.A. Chandler, K.D. Hahn, M.J. Moran, M.B. Schneider, N.E. Palmer, R.M. Bionta, E.P. Hartouni, S. LePape, P.K. Patel, N. Izumi, R. Tommasini, E.J. Bond, J.A. Caggiano, R. Hatarik, G.P. Grim, F.E. Merrill, D.N. Fittinghoff, N. Guler, O. Drury, D.C. Wilson, H.W. Herrmann, W. Stoeffl, D.T. Casey, M.G. Johnson, J.A. Frenje, R.D. Petrasso, A. Zylestra, H. Rinderknecht, D.H. Kalantar, J.M. Dzenitis, P. Di Nicola, D.C. Eder, W.H. Courdin, G. Gururangan, S.C. Burkhart, S. Friedrich, D.L. Blueuel, L.A. Bernstein, M.J. Eckart, D.H. Munro, S.P. Hatchett, A.G. Macphee, D.H. Edgell, D.K. Bradley, P.M. Bell, S.M. Glenn, N. Simanovskaia, M.A. Barrios, R. Benedetti, G.A. Kryala, R.P.J. Town, E.L. Dewald, J.L. Milovich, K. Widmann, A.S. Moore, G. LaCaille, S.P. Regan, L.J. Suter, B. Felker, R.C. Ashabranner, M.C. Jackson, R. Prasad, M.J. Richardson, T.R. Kohut, P.S. Datte, G.W. Krauter, J.J. Klingman, R.F. Burr, T.A. Land, M.R. Hermann, D.A. Latray, R.L. Saunders, S. Weaver, S.J. Cohen, L. Berzins, S.G. Brass, E.S. Palma, R.R. Lowe-Webb, G.N. McHalle, P.A. Arnold, L.I. Lagin, C.D. Marshall, G.K. Brunton, D.G. Mathisen, R.D. Wood, J.R. Cox, R.B. Ehrlich, K.M. Knittel, M.W. Bowers, R.A. Zacharias, B.K. Young, J.P. Holder, J.R. Kimbrough, T. Ma, K.N. La Fortune, C.C. Widmayer, M.J. Shaw, G.V. Erbert, K.S. Jancaitis, J.M. DiNicola, C. Orth, G. Heestand, R. Kirkwood, C. Haynam, P.J. Wegner, P.K. Whitman, A. Hamza, E.G. Dzenitis, R.J. Wallace, S.D. Bhandarkar, T.G. Parham, R. Dylla-Spears, E.R. Mapoles, B.J. Kozioziemski, J.D. Sater, C.F. Walters, B.J. Haid, J. Fair, A. Nikroo, E. Giraldez, K. Moreno, B. Vanwonterghem, R.L. Kauffman, S. Batha,

D.W. Larson, R.J. Fortner, D.H. Schneider, J.D. Lindl, R.W. Patterson, L.J. Atherton, and E.I. Moses, Phys. Rev. Lett. **108**, 215005 (2012).

[20]H.W. Herrmann, N. Hoffman, D.C. Wilson, W. Stoeffl, L. Dauffy, Y.H. Kim, A. McEvoy, C.S. Young, J.M. Mack, C.J. Horsfield, M. Rubery, E.K. Miller, and Z.A. Ali, Rev. Sci. Instrum. **81**, 10D333 (2010).

[21]A.T. Anderson, R.A. Managan, M.T. Tobin, and P.F. Peterson, Fusion Technol. **30**, 425 (1996).

[22]B.E. Blue, J.F. Hansen, M.T. Tobin, D.C. Eder, and H.F. Robey, Rev. Sci. Instrum. **75**, 4775 (2004).

[23]D. Eder, A. Koniges, F. Bonneau, J. Vierne, P. Combis, M. Tobin, J. Andrews, K. Mann, and B. MacGowan, in *Inertial Fusion Sciences and Applications*, edited by B.A. Hammel, D.D. Meyerhofer, J. Meyer-ter-Vehn and H. Azechi (American Nuclear Society, La Grange Park, IL, 2004), p. 572.

[24]F.E. Irons and N.J. Peacock, J. Phys. B **7**, 2084 (1974).

[25]M. Dombrowski and W.R. Jones, Chem. Engineering Sci. **18**, 203 (1963).

[26]D.C. Eder, A.E. Koniges, O.S. Jones, M.M. Marinak, M.T. Tobin, and B.J. MacGowan, Nucl. Fusion **44**, 709 (2004).

[27]D.C. Eder, A.E. Koniges, O.L. Landen, N.D. Masters, A.C. Fisher, O.S. Jones, T.I. Suratwala, and L.J. Suter, J. Phys. Conf. Ser. **112**, 032023 (2008).

[28]J.M. Gostic, D.A. Shaughnessy, K.T. Moore, I.D. Hutcheon, P.M. Grant, and K.J. Moody, Rev. Sci. Instrum. **83**, 10D904 (2012).

[29]J.H. Hubbell and S.M. Seltzer, *Tables of X-Ray Mass Attenuation Coefficients and Mass Energy-Absorption Coefficients (version 1.4)* (National Institute of Standards and Technology, Gaithersburg, MD, 2004), http://physics.nist.gov/zaamdi.

[30]Y.S. Touloukian, R.W. Powell, C.Y. Ho, and M.C. Nicolaou, *Thermal Diffusivity* (IFI/Plenum, New York, 1973).

[31]A.M. Hassanein, H.M. Attaya, and G.L. Kulcinski, Journ. Nucl. Mat. **141**, 221 (1986).

[32]D.C. Eder, R.W. Anderson, D.S. Bailey, P. Bell, D.J. Benson, A.L. Bertozzi, W. Bittle, D. Bradley, C.G. Brown, T.J. Clancy, H. Chen, J.M. Chevalier, P. Combis, L. Dauffy, C.S. Debonnel, M.J. Eckart, A.C. Fisher, A. Geille, V.Y. Glebov, J. Holder, J.P. Jadaud, O. Jones, T.B. Kaiser, D. Kalantar, H. Khater, J. Kimbrough, A.E. Koniges, O.L. Landen, B.J. MacGowan, N.D. Masters, A. MacPhee, B.R. Maddox, M. Meyers, S. Osher, R. Prasad, D. Raffestin, J. Raimbourg, V. Rekow, C. Sangster, P. Song, C. Stoeckl, M.L. Stowell, J.M. Teran, A. Throop, R. Tommasini, J. Vierne, D. White, and P. Whitman, J. Phys. Conf. Ser. **244**, 032018 (2010).

[33]J.A. Frenje, D.T. Casey, C.K. Li, F.H. Seguin, R.D. Petrasso, V.Yu. Glebov, P.B. Radha, T.C. Sangster, D.D. Meyerhofer, S.P. Hatchett, S.W. Haan, C.J. Cerjan, O.L. Landen, K.A. Fletcher, and R.J. Leeper, Phys. Plasmas **17**, 056311 (2010).

[34]C. Stoeckl, M. Cruz, V.Yu. Glebov, J.P. Knauer, R. Lauck, K. Marshall, C. Mileham, T.C. Sangster, and W. Theobald, Rev. Sci. Instrum. **81**, 10D302 (2010).

[35]R.A. Lerche, V.Yu. Glebov, M.J. Moran, J.M. McNaney, J.D. Kilkenny, M.J. Eckart, R.A. Zacharias, J.J. Haslam, T.J. Clancy, M.F. Yeoman, D.P. Warwas, T.C. Sangster, C. Stoeckl, J.P. Knauer, and C.J. Horsfield, Rev. Sci. Instrum. **81**, 10D319 (2010).

[36]V.Yu. Glebov, D.D. Meyerhofer, T.C. Sangster, C. Stoeckl, S. Roberts, C.A. Barrera, J.R. Celeste, C.J. Cerjan, L.S. Dauffy, D.C. Eder, R.L. Griffith, S.W. Haan, B.A. Hammel, S.P. Hatchett, N. Izumi, J.R. Kimbrough, J.A. Koch, O.L. Landen, R.A. Lerche, B.J. MacGowan, M.J. Moran, E.W. Ng, T.W. Phillips, P.M. Song, R. Tommasini, B.K. Young, S.E. Caldwell, G.P. Grim, S.C. Evans, J.M. Mack, T.J. Sedillo, M.D. Wilke, D.C. Wilson, C.S. Young, D. Casey, J.A. Frenje, C.K. Li, R.D. Petrasso, F.H. Séguin, J.L. Bourgade, L. Disdier, M. Houry, I. Lantuejoul, O. Landoas, G.A. Chandler, G.W. Cooper, R.J. Leeper, R.E. Olson, C.L. Ruiz, M.A. Sweeney, S.P. Padalino, C. Horsfield, and B.A. Davis, Rev. Sci. Instrum. **77**, 10E715 (2006).

[37]V.Yu. Glebov, T.C. Sangster, C. Stoeckl, J.P. Knauer, W. Theobald, K.L. Marshall, M.J. Shoup III, T. Buczek, M. Cruz, T. Duffy, M. Romanofsky, M. Fox, A. Pruyne, M.J. Moran, R.A. Lerche, J. McNaney, J.D. Kilkenny, M.J. Eckart, D. Schneider, D. Munro, W. Stoeffl, R. Zacharias, J.J. Haslam, T. Clancy, M. Yeoman, D. Warwas, C.J. Horsfield, J.-L. Bourgade, O. Landoas, L. Disdier, G.A. Chandler, and R.J. Leeper, Rev. Sci. Instrum. **81**, 10D325 (2010).

[38]J.A. Frenje, R. Bionta, E.J. Bond, J.A. Caggiano, D.T. Casey, C. Cerjan, J. Edwards, M. Eckart, D.N. Fittinghoff, S. Friedrich, V.Yu. Glebov, S. Glenzer, G. Grim, S. Haan, R. Hatarik, S. Hatchett, M. Gatu Johnson, O.S. Jones, J.D. Kilkenny, J.P. Knauer, O. Landen, R. Leeper, S. Le Pape, R. Lerche, C.K. Li, A. Mackinnon, J. McNaney, F.E. Merrill, M. Moran, D.H. Munro, T.J. Murphy, R.D. Petrasso, R. Rygg, T.C. Sangster, F.H. Séguin, S. Sepke, B. Spears, P. Springer, C. Stoeckl, and D.C. Wilson, Nucl. Fusion **53**, 043014 (2013).

[39]D. Drake, I. Bergqvist, and D.K. McDaniels, Phys. Lett. B **36**, 557 (1971).

[40]MCNP—A General N-Particle Transport Code, Volume 5, X-5 Monte Carlo Team, LA-UR-03-1987 (2003, updated 2008).

[41]H. Xiaolong, Nucl. Data Sheets **110**, 2533 (2009).

[42]H. Xiaolong, Nucl. Data Sheets **108**, 1093 (2007).

[43]R.B. Firestone and V.S. Shirley, editors, *Table of Isotopes, 8th edition*, volume 2, (John Wiley and Sons, New York, 1996).

[44]G. Audi, O. Bersillon, J. Blachot, and A.H. Wapstra, Nucl. Phys. A **729**, 3 (2003).

[45]B.P. Bayhurst, J.S. Gilmore, R.J. Prestwood, J.B. Wilhelmy, N. Jarmie, B.H. Erkkila, and R.A. Hardekopf, Phys. Rev. C **12**, 451 (1975).

[46]R.J. Prestwood and B.P. Bayhurst, Phys. Rev. **121**, 1438 (1961).

[47]W. Dilg, H. Vonach, G. Winkler, and P. Hille, Nucl. Phys. A **118**, 9 (1968).

[48]G.N. Flerov, Yu.P. Gangrskii, B.N. Markov, A.A. Pleve, S.M. Polikanov, and Kh. Yungklaussen, Sov. J. Nucl. Phys. **6**, 12 (1968).

[49]R.B. Ryves and P. Kolkowski, J. Phys. G **7**, 115 (1981).

[50]M.B. Chadwick, M. Herman, P. Obložinský, M.E. Dunn, Y. Danon, A.C. Kahler, D.L. Smith, B. Pritychenko, G. Arbanas, R. Arcilla, R. Brewer, D.A. Brown, R. Capote, A.D. Carlson, Y.S. Cho, H. Derrien, K. Guber, G.M. Hale, S. Hoblit, S. Holloway, T.D. Johnson, T. Kawano, B.C. Kiedrowski, H. Kim, S. Kunieda, N.M. Larson, L. Leal, J.P. Lestone, R.C. Little, E.A. McCutchan, R.E. MacFarlane, M. MacInnes, C.M. Mattoon, R.D. McKnight, S.F. Mughabghab, G.P.A. Nobre, G. Palmiotti, A. Palumbo, M.T. Pigni, V.G. Pronyaev, R.O. Sayer, A.A. Sonzogni, N.C. Summers, P. Talou, I.J. Thompson, A. Trkov, R.L. Vogt, S.C. van der Marck, A. Wallner, M.C. White, D. Wiarda, and P.G. Young, Nucl. Data Sheets **112**, 2887 (2011).

[51]G. Magnussen, P. Andersson, and I. Bergqvist, Phys. Scripta **21**, 21 (1980).

[52]O. Schwerer, M. Winkler-Rohatsch, H. Warhanek, and G. Winkler, Nucl. Phys. A **264**, 105 (1976).

[53]R. Plummer, "Diagnostic Instrument Manipulator (DIM) upgrades for reliability and operational efficiency in a radiological contamination environment at the National Ignition Facility (NIF)", *Target Diagnostics Physics and Engineering for Inertial Confinement Fusion II*, edited by P.M. Bell and G.P. Grim, SPIE Vol. 8850, 885005 (2013).

[54]G.F. Knoll, *Radiation detection and measurement*, *3rd edition,* (Wiley, New York, 2000).

[55]C.M. Davisson in *Alpha-, Beta- and Gamma-Ray Spectroscopy*, edited by K. Siegbahn (North-Holland, Amsterdam, 1965).

[56]*Nuclear Counting Facility Detector Calibration Procedure for the Forensic Science Center*, FSC-SOP-26, rev. 4 (LLNL-TM-427812).

[57]R. Gunnink and J.B. Niday, *Computerized quantitative analysis by gamma-ray spectrometer*, Lawrence Livermore Laboratory report UCRL-57061 (1971).

[58]R. Gunnink and J.B. Niday, in *ERDA symposium on X- and gamma-ray sources and applications*, (U. S. Energy Research and Development Administration, CONF-760539, Washington, DC., GPO, 1976).

[59]Z.A. Ali, V.Yu. Glebov, M. Cruz, T. Duffy, C. Stoeckl, S. Roberts, T.C. Sangster, R. Tommasini, A. Throop, M. Moran, L. Dauffy, and C. Horsfield, Rev. Sci. Intrum. **79**, 10E527 (2008).

[60]J.A. Frenje, D.T. Casey, C.K. Li, J.R. Rygg, F.H. Seguin, R.D. Petrasso, V.Y. Glebov, D.D. Meyerhofer, T.C. Sangster, S. Hatchett, S. Haan, C. Cerjan, O. Landen, M. Moran, P. Song, D.C. Wilson, and R.J. Leeper, Rev. Sci. Instrum. **79**, 10E502 (2008).

[61]M. Busso, R. Gallino, and G.J. Wasserberg, Ann. Rev. Astron. Astrophys. **37**, 239 (1999).

[62]F. Kaeppeler, R. Gallino, S. Bisterzo, and A. Wako, Rev. Mod. Phys. **83**, 157 (2011).

[63]V. Trimble, Rev. Mod. Phys. **47**, 877 (1975).